Journal of King Saud University – Engineering Sciences (2016) 28, 123–129

King Saud University

Journal of King Saud University – Engineering Sciences

www.ksu.edu.sa
www.sciencedirect.com

ORIGINAL ARTICLE

Hydrothermal formation and electrochemical property of $Ag_{1.8}Mn_8O_{16}$ microcrystals for Li-ion battery cathode application

Khalid Abdelazez Mohamed Ahmed [a,b,*], **Kaixun Huang** [c]

[a] *Department of Chemistry, Faculty of Science and Education, Taif University, P.O. Box 888, Postal Code: 5700, Saudi Arabia*
[b] *Department of Chemistry, Faculty of Science and Technology, Al-Neelain University, P.O. Box 12702, Khartoum, Sudan*
[c] *School of Chemistry and Chemical Engineering, Huazhong University of Science and Technology, Wuhan 430074, PR China*

Received 27 November 2013; accepted 18 March 2014
Available online 27 March 2014

KEYWORDS

Silver manganese oxide;
Microcrystals;
Hydrothermal;
Characterization;
Li-ion battery

Abstract In this article, $Ag_{1.8}Mn_8O_{16}$ microcrystals assembled from nanosphere building blocks were successfully fabricated via a one-pot hydrothermal route using silver nitrate and potassium permanganate as raw materials. The particles were characterized by X-ray powder diffraction (XRD), energy dispersive X-ray microanalysis (EDX), field emission scanning electron microscopy (FE-SEM), transmission electron microscopy (TEM), high-resolution transmission electron microscopy (HR-TEM), cyclic voltammogram, galvanostatic charge–discharge and Nyquist plane plot. Ordinary differential equations (ODEs) and the electrode kinetics were used to investigate the synthesis and electrochemical activity. The as-prepared $Ag_{1.8}Mn_8O_{16}$ microspheres reveal the highest reversible discharge capacity ~1468 mAh even after 100 cycles in the potential range of 3.4–4.2 V and the best cycling stability.

1. Introduction

Rechargeable Li-ion batteries are widely used in multifarious applications which include portable electronic devices, toys, mobile phones, laptop, watches ... etc. They are also expected to power electric vehicles in the near future due to their ability to provide fast response to energy demand, ease for sitting and their high energy efficiency (Aronson et al., 1999; Choi et al., 2012; Cairns and Albertus, 2010). Micro/nanometer-scale materials often exhibit intriguing physical and chemical properties that are rarely present in bulk materials. The controlled synthesis of inorganic micro- nanostructures with well-defined shapes and sizes has attracted increasing interest because of their widespread potential applications, including batteries (Lou et al., 2008; Wu et al., 2006; Zeng et al., 2007), sensors (Wingert et al., 2007; Zhao et al., 2006; Gao et al., 2008), catalysis (Yu et al., 2007; Li et al., 2007), drug delivery (Zhu et al., 2005; Cai et al., 2007; Ma et al., 2008), and biomedical imaging

* Corresponding author at: Department of Chemistry, Faculty of Science and Education, Taif University, P.O. Box 888, Postal Code: 5700, Saudi Arabia. Tel.: +966 552639984.
E-mail address: khalidgnad@hotmail.com (K.A.M. Ahmed).

Peer review under responsibility of King Saud University.

ELSEVIER Production and hosting by Elsevier

http://dx.doi.org/10.1016/j.jksues.2014.03.004

(Chen et al., 2005; Caruso et al., 1998; Lou et al., 2008). In recent years, great effort has been exercised to fabricate nanomaterials with different shapes. The simplest synthetic method to obtain these structures is probably self-assembly, in which ordered aggregates are formed in a spontaneous process.

Among different kinds of transition metal oxides, manganese oxide nanomaterials are of great importance in magnetic, catalyst, ion-exchange material, electrochemistry and batteries (Vries et al., 2002; Ma et al., 2004; Han et al., 2006; Zhu et al., 2008; Ragupathy et al., 2010). More recent battery research and development have focused on rechargeable lithium and lithium-ion battery chemistries, which offer the advantages of higher voltages and higher energy densities with the ever-increasing power and energy needs of advanced consumer electronics and related technologies (Thackeray, 1997; Benhaddad et al., 2009; Messaoudi et al., 2001). The intense interest in manganese oxides for battery applications is driven by their low cost and low toxicity, particularly when compared to other metal oxides of relevance for batteries such as nickel- and cobalt-oxides. They have a relatively long history in the world of battery chemistry, dating back to the work of Leclanché in the 1860s, which ultimately formed the basis for the now-ubiquitous primary alkaline cell (Bélanger et al., 2008). As a general class of materials, manganese oxides exhibit a very rich chemistry and can be synthesized in dozens of crystalline and disordered forms, each with distinctive physical and electrochemical characteristics (Nagaraju et al., 2008; Ma et al., 2007. However, the selection of transition metal ions incorporated in the framework of manganese oxides can improve the conductivity properties of the semiconductor material (Brousse et al., 2004; Yin et al., 2011; Sawangphruk et al., 2012; Zhang et al., 2004). The doping elements such as bismuth, vanadium, magnesium and cobalt into manganese oxides to be introduced serve to vary the conductivity properties of the semiconductor material (Nakayama et al., 2005; Bach et al., 1995; Hashem et al., 2011; Aronson et al., 1999; Tsuda et al., 2002). Dopant metal such as silver into birnessite not only stabilizes the layer structure but also it increased the conductivity efficiency (Ahn et al., 2008).

Herein, in this paper, we report the preparation of $Ag_{1.8}Mn_8O_{16}$ microcrystals assembled from nanosphere building blocks for the first time using the simple hydrothermal route. The varieties of techniques were employed to estimate the crystal structure, morphology and electrochemical property of product. Based on the time dependent experiments, we note that the formation of the as-prepared microstructure can be accompanied by the Ostwald ripening process and recrystallization mechanisms. Their electrochemical property of $Ag_{1.8}Mn_8O_{16}$ microcrystals as cathode material for lithium ion battery has been addressed. ODEs and the electrode kinetics theoretic were also estimated.

2. Experimental section

2.1. Synthesis and characterization of the sample

For the synthesis of silver manganese oxide microcrystal, all chemicals were of analytical grade from Shanghai Chemical Reagents Co., China. In the typical synthesis process, 1 mmol of $KMnO_4$ and 0.25 mmol of $AgNO_3$ were dissolved in 35 ml deionization water. The solution was stirred for 10 min at room temperature and then transferred into a 40 ml Teflon-lined stainless steel autoclave sealed at 140 °C for 14 h. The autoclave was cooled to room temperature naturally when the reaction time was finished. The product was collected by centrifugation at 8000 rpm for 5 min and washed with distilled water and absolute ethanol several times to remove the excessive reactants and byproducts, followed by drying in a vacuum at 50 °C for 24 h.

Characterization techniques such as X-ray diffraction (XRD, Panalytical χ'Pert Pro., Netherlands), use a Cu target (CuK_α = 1.5418) at an angular 2θ speed of 2° per minute. EDAX Eagle III energy-dispersive micro-XRF (mXRF) spectrometer was used to identify the elements present. Field emission scanning electron microscope (FESEM) observations were performed on a FEI Sirion 200. Transmission electron microscopy (TEM) images were collected using a Tecnai G220, Netherlands. High-resolution transmission electron microscopy (HR-TEM) images were carried out on a JEM-2010 FEF TEM.

2.2. Electrochemical measurements

Electrochemical characterizations were carried in lithium foil was used as both the counter and the reference electrodes. The composite electrodes were prepared by 80% silver manganese oxide powder and acetylene black 10% was mixed with 10% poly(tetrafluoroethylene) (PTFE) binder in ethanol solvent. The composite material was mixed and pressed with a twin roller and then dried under vacuum at 60 °C for 24 h. Finally, the cathode was prepared by pressing the composite into film. The electrolyte solution of 1 M $LiClO_4$ was dissolved in ethylene carbonate (EC) and a (1:1 by volume) mixture of EC and diethylene carbonate (DEC), respectively. Because lithium is very sensitive to oxygen and causes fire, the cell must be fully purged and refilled with argon gas. The galvanostatic charge–discharges were measured in the voltage of 3.4–4.2 V.

3. Results and discussion

3.1. Morphology and structure

Fig. 1(a) shows the typical powder XRD pattern of the as-synthesized product. Diffraction peaks are assigned to $Ag_{1.8}Mn_8$-

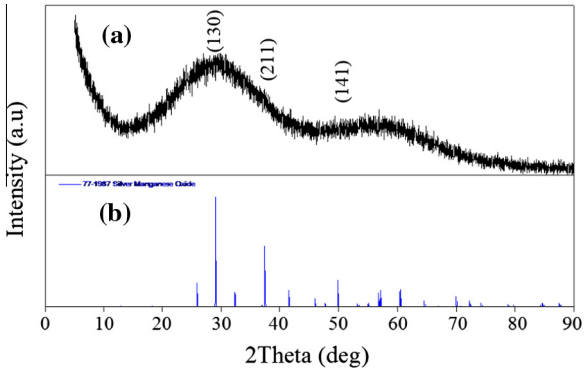

Figure 1 (a) XRD pattern of $Ag_{1.8}Mn_8O_{16}$ product synthesized by hydrothermal process at 140 °C for 14 h and (b) the standard data from JCPDS card No. 18–0802.

O_{16} tetrahedral structure with lattice parameter of $a = 9.725$ and $c = 2.885$ (JCPDS No.77–1987) (Fig. 1(b)). The interpretation of the powder X-ray diffraction data is often limited to the analysis of the reflection position and the comparison between the interlayer distance and the size of the intercalated molecule, so EDAX spectra occurred in Fig. 2. From figure, the ratio of Ag to Mn elements is about 0.8:1. The peaks at 2.98 and 3.16 keV results are attributed from $AgL_{\alpha 1}$ and $AgL_{\beta 1}$, respectively. Furthermore, the peaks at 5.90 and 6.5 keV represented the $MnK_{\alpha 1}$, and $MnK_{\beta 1}$, respectively. The crystal structure of silver manganese oxide (insert a Fig. 2) shows MnO_6 octahedra and O–Ag–O sticks (Koriche et al., 2007).

Fig. 3(a) shows the typical field emission scanning electron microscopy (SEM) images of the surface of $Ag_{1.8}Mn_8O_{16}$ microcrystals. It is found from figure, the edge size of microcrystals is about 5.5 μm and length around 10.5 μm. Fig. 3(b) shows the high panoramic SEM image of $Ag_{1.8}Mn_8O_{16}$. The close-up SEM image in figure shows that the sample okra-like crystal consisted of microspheres in the inner side. The microsphere has a diameter size of 1–1.5 μm. The morphology of microcrystal is also investigated by TEM images (Fig. 3(c)), which is in agreement with the FE-SEM observa-

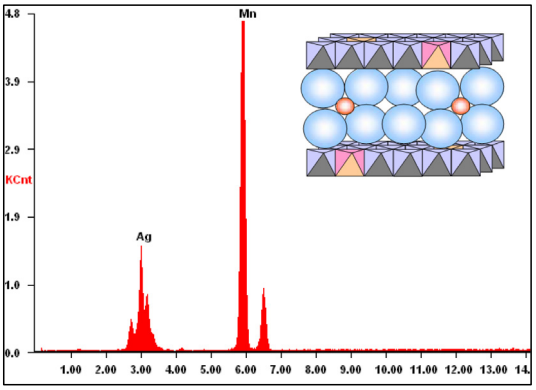

Element	*Wt%*	*At%*
AgL	38.84	15.51
MnK	61.16	84.49
AgK	00.00	00.00

Figure 2 EDAX spectrum of $Ag_{1.8}Mn_8O_{16}$ sample by hydrothermal process at 140 °C for 14 h.

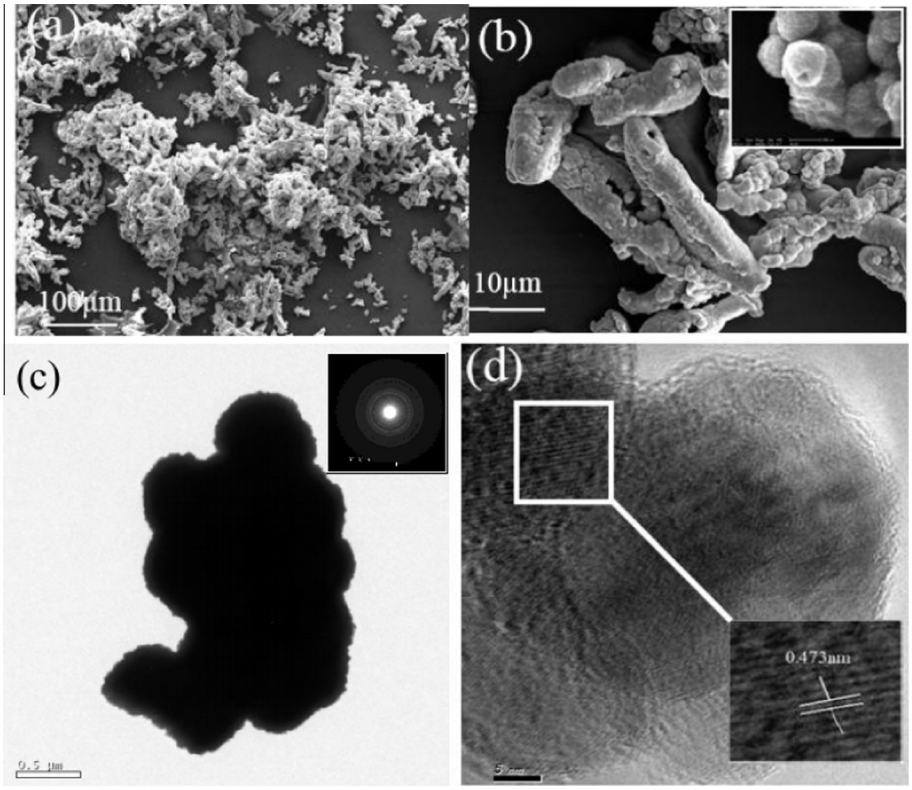

Figure 3 (a) Low- and (b) high-magnification of FE-SEM images; (c) TEM and SAED (inset) patterns; (d) HR-TEM images of the as-prepared $Ag_{1.8}Mn_8O_{16}$ microsrystals.

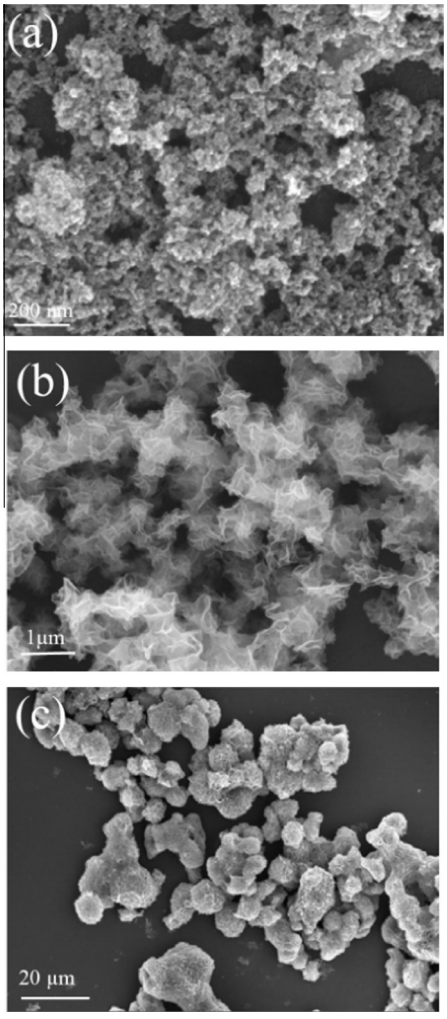

Figure 4 FE-SEM image of the as-prepared samples by hydrothermal route at 140 °C for different times (a) 5 h, (b) 8 h and (c) 10 h.

tion. It also indicates that the samples consist of many $Ag_{1.8}Mn_8O_{16}$ microspheres. The selected area electron diffraction (SA-ED) pattern inserted in Fig. 3(c) shows that product has a polycrystalline structure. The HR-TEM crystallographic analysis in Fig. 3(d), reveals interplanar spacing of the lattice fringes is 0.473 nm, corresponding to the {200} plane of tetrahedral silver manganese oxide.

To thoroughly investigate the evolution process of the microstructures, time-dependent experiments were carried out by keeping all other conditions constant. Small particle crystals precipitate with an average size 50–60 nm when the reaction time is following for 5 h (Fig. 4(a)). When the time is increased to 8 h, the product collected together to form hierarchical like microstructure on liquid phase precipitates (Fig. 4(b)). When the reaction time is prolonged to 10 h, the hierarchical structures are converted to spherical-like structures (Fig. 4(c)). Based on the above experimental results and reports in the literature Ma et al., 2011; Bao et al., 2007, suggest that the formation of silver manganese oxide microspheres maybe accompanied by the Ostwald ripening process and re-crystallization mechanisms. Owing to the energy difference, Ostwald ripening includes the formation of aggregates with primary crystallites, followed by the gradual migration of crystallites through a re-crystallization process. A three-step growth model is proposed to display the formation of such a sphere nanostructure. In the first step, the potassium permanganate was reduced by water to obtain K-birnessite particles. In the second step, the particles appeared in the solution, and they might act as the primary particles for the formation of sphere particle structure. Then sphere crystallites of the aggregate went to the solid silver manganese oxide microcrystals by ionic exchange as in the third step. Due to dissolution re-crystallization process, the hole of microstructures may have occurred.

3.2. Electrochemical application

The electrochemical performances of the as-prepared silver manganese oxide microspheres were studied subsequently. The galvanostatic charge/discharge curves of the initial voltage profiles of the silver manganese oxide electrodes with excessive lithium content x are probed in $LiClO_4$ electrolyte under a charge–discharge current density of 0.2 mA and potential range of 3.4–4.2 V (Fig. 5(a)). The initial discharge and charge

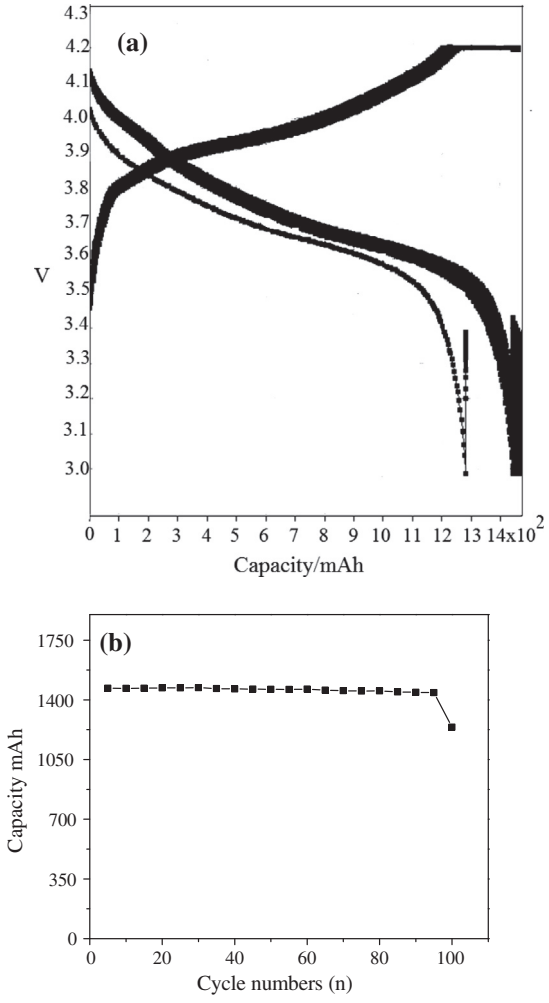

Figure 5 (a) Discharge–charge voltage profiles and (b) specific capacities of $Ag_{1.8}Mn_8O_{16}$ microcrystals.

specific capacity are 1468 and 1239 mAh, respectively. The CV curves are shown in Fig. 5(b), reveals that the discharge specific capacity exhibits slight drop after every discharge cycle the discharge specific capacity at the 100th cycle is still remain of 1239 mAh. This result is better than that prepared of undoped material such as KMn_8O_{16} nanorods (Zheng et al., 2013) and it also indicates that the silver manganese oxide composite has a good cycling behavior and electrochemical impedance technique. As illustrated in Fig. 6(a), the cyclic voltammograms of silver manganese oxide microspheres have evidenced for the intercalation–deintercalation process of cathode material which may be as follows:

$$x\ \mathrm{Li}^+ + \text{Silver manganese oxide} + \mathrm{xe}^- \leftrightarrow \mathrm{Li}_x \text{ silver manganese oxide}$$

The electrode voltage can be affected on rate of the electron transfer is increased the reaction rate and therefore the current will increase exponentially means that the possible to pass unlimited quantities of current. Of course in reality this does not arise and this can be rationalized by considering the expression for the current that we encountered in the electrode kinetics section: $\{i_c = -nFAk_{red}[O]_o\}$; where (A) is electrode area, k_{red} rate constant and $[O]_o$ the surface concentration of the reactant. Nyquist plane plot of the as-prepared material is exhibited in Fig. 6(b), nearly straight line characteristic of a diffusion-limiting step in the electrochemical process. The mid-frequency semicircle is considered as the charge-transfer impedance on electrode–electrolyte interface with less resistance. However, the capacity is much higher than the incorporation metals such as magnesium and cobalt into birnessite electrodes (Aronson et al., 1999; Tsuda et al., 2002). Additive elements such as cobalt, vanadium, carbon black or Nafion into birnessite can improve the cycle ability of the material activity even at a high rate, owing to the enhanced electrical or ionic conductivity (Matsuo et al., 2005; Liang et al., 2004; Yang et al., 2002). Recently studies the conductivity of manganese dioxide can significantly be increased by the morphology phase and Ag additive in framework of manganese dioxide are affected on the electrochemical capacitor of Li ion battery (Ahn et al., 2008). In non-equilibrium hydrothermal dynamics, chemical reactions between the constituent reactors must be modeled along with the thermodynamics, required in certain regimes of hypersonic aerodynamic modeling. Hence restricting our attention to in method condition, we have essentially the Euler equations of solution dynamics, coupled with source terms representing the chemistry. In two space dimensions these equations take the form (LeVeque and Yee, 1990):

$$u_t + f(u)_x + g(u)_y = \Psi(u) \tag{1}$$

where u is the vector of dependent variables including momentum, energy, and concentrations for each species in the reacting mixture; f and g describe the dynamics as in the Euler equations while the source term $\Psi(u)$ arises from the chemistry of the reacting species. The classical participate of ordinary differential equations (ODEs) arises in modeling chemical kinetics with uniform stirred reactor where the hydrodynamics terms drop out given:

$$u_t + u_x = \Psi(u) \tag{2}$$

With

$$\Psi(u) = \mu u(u-1)(u-1/2) \tag{3}$$

This is the linear advection equation with a source term that is stiff for large μ. Along the characteristic $x = x_o + t$, the solution to (2) evolves according to the ODE.

$$(d/dt)u(x_o + t, t) = \Psi[u(x_o + t, t)] \tag{4}$$

with initial data $u(x_o,0)$. This equation has stable equilibria at $u = 0$ and $u = 1$ and an unstable equilibrium at $u = 1/2$. For large p and arbitrary initial data the ODE solution consists of a rapid transient with u approaching 0 (if $u(x_o,0) < 1/2$) or 1 (if $u(x_o,0) > 1/2$). $\Psi(u)$ could also be considered. The model corresponding is more closely to ignition temperature kinetics.

$$\Psi(u) = \begin{cases} -\mu(u-1) & \text{if } u > 1/2 \\ 0 & \text{if } u < 1/2 \end{cases}$$

According to ODE controller, the energy conversion is the simultaneous shuttling of electrons to and from electrodes via complementary chemical reactions. During discharge, electrons are delivered from the cathode through an electrolyte medium by reduction and oxidation reaction is given good electrochemical characterization. On the other hand, XRD analysis and FE-SEM images of the as-prepared cathode were investigated. Fig. 7 shows the morphology and structure of as-

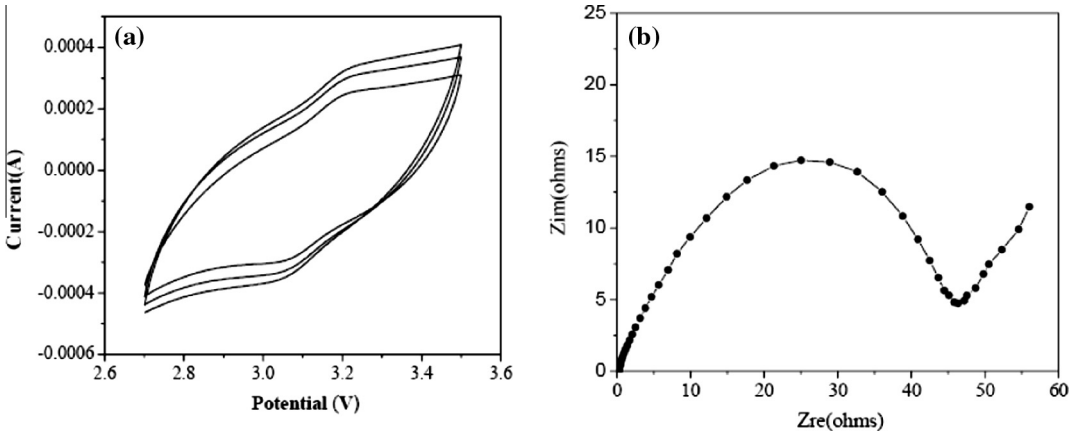

Figure 6 (a) Cyclic voltammogram and (b) Nyquist plot of $Ag_{1.8}Mn_8O_{16}$ microcrystals at a scan rate of 0.2 mV/s in a $LiClO_4$ electrolyte.

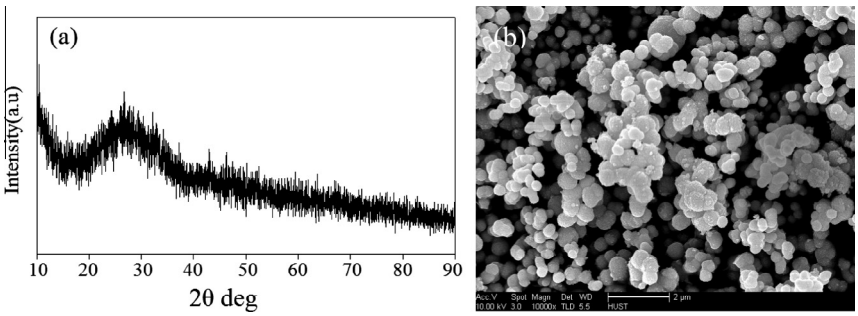

Figure 7 (a) XRD pattern and (b) FE-SEM images on the activity of the prepared cathode.

synthesized cathode is changed by additive materials such as acetylene black and PTFE. These results confirm that silver may increase the manganese oxide skeleton and conductive ability. The excellent electrochemical performances of silver manganese oxide microspheres cathode materials are attributed to the peculiar structures. The particle structures reduce Li^+ diffusion length and improve the ionic diffusion.

4. Conclusion

In summary, silver manganese oxide microcrystals were prepared by hydrothermal reaction. The morphology of $Ag_{1.8}Mn_8O_{16}$ microcrystals is okra-like crystal in shape consisting of microspheres in the inner side. The Ostwald ripening process and re-crystallization mechanisms were suggested to address the formation of the as-prepared microstructure. The silver manganese oxide microcrystals showed the highest discharge capacity, best electrochemical performance, and high rate capability. After 100 cycles, the electrode exhibited a reversible discharge capacity up to 1468 mAh with a current density of 0.2 mA. Also ordinary differential equations (ODEs) dependent variables including momentum, energy and concentrations for each species in the reacting mixture are predicted a good electrochemical characterization of this material.

Acknowledgements

The author kindly acknowledges the financial support from the Vice-Presidency of Graduate Studies and Academic Research; Taif University (project 1-435-2998). This research also was supported in part by grants from Huazhong University of Science and Technology (Project No. 2006CB705606a).

Reference

Ahn, H.J., Sung, Y.E., Kim, W.B., Seong, T.Y., 2008. Crystalline Ag nanocluster-incorporated RuO_2 as an electrode material for thin-film micropseudocapacitors. Electrochem. Solid-State Lett. 11, A112–A115.

Aronson, B.J., Kinser, A.K., Passerini, S., Smyl, W.H., Stein, A., 1999. Synthesis, characterization, and electrochemical properties of zinc and magnesium birnessites prepared by a low temperature route. Chem. Mater. 11, 949–957.

Bach, S., Pereira-Ramos, J.-P., Cachet, C., Bode, M., Yu, L.T., 1995. Effect of Bi-doping on the electrochemical behaviour of layered MnO_2 as lithium intercalation compound. Electrochim. Acta 40, 785–789.

Bao, S.J., Bao, Q.L., Li, C.M., Chen, T.P., Sun, C.Q., Dong, Z.L., Gan, Y., Zhang, J., 2007. Synthesis and electrical transport of novel channel-structured β-$AgVO_3$. Small 3, 1174–1177.

Bélanger, D., Brousse, T., Long, J.W., 2008. Manganese oxides: battery materials make the leap to electrochemical capacitors. Electrochem. Soc. Interface 17 (1), 49–52.

Benhaddad, L., Makhloufi, L., Messaoudi, B., Rahmouni, K., Takenouti, H., 2009. Reactivity of nanostructured MnO_2 in alkaline medium studied with a microcavity electrode: effect of synthesizing temperature. Appl. Mater. Interface 1, 424–432.

Brousse, T., Toupin, M., Belanger, D., 2004. A hybrid activated carbon-manganese dioxide capacitor using a mild aqueous electrolyte. J. Electrochem. Soc. 151, 614A–622A.

Cai, Y., Pan, H., Xu, X., Hu, Q., Li, L., Tang, R., 2007. Ultrasonic controlled morphology transformation of hollow calcium phosphate nanospheres: a smart and biocompatible drug release system. Chem. Mater. 19, 3081–3083.

Cairns, E.J., Albertus, P., 2010. Batteries for electric and hybrid-electric vehicles. Annu. Rev. Chem. Biomol. Eng. 1, 299–320.

Caruso, F., Caruso, R.A., Mohwald, H., 1998. Nanoengineering of inorganic and hybrid hollow spheres by colloidal templating. Science 282, 1111–1114.

Chen, J., Saeki, F., Wiley, B.J., Cang, H., Cobb, M.J., Li, Z.Y., Au, L., Zhang, H., Kimmey, M.B., Li, X., Xia, Y., 2005. Gold nanocages: bioconjugation and their potential use as optical imaging contrast agents. Nano Lett. 5, 473–477.

Choi, N.-S., Chen, Z., Freunberger, S.A., Yushin, G., Ji, X., Sun, Y.-K., Amine, K., Nazar, L.F., Cho, J., Bruce, P.G., 2012. Challenges facing lithium batteries and electrical double-layer capacitors. Angew. Chem. Int. Ed. 51, 9994–10024.

Gao, J., Li, Q., Zhao, H., Li, L., Liu, C., Gong, Q., Qi, L., 2008. One-pot synthesis of uniform Cu_2O and CuS hollow spheres and their optical limiting properties. Chem. Mater. 20, 6263–6269.

Han, Y.F., Chen, F.X., Zhong, Z.Y., Ramesh, K., Chen, L.W., Widjaja, E., 2006. Controlled synthesis, characterization, and catalytic properties of Mn_2O_3 and Mn_3O_4 nanoparticles supported on mesoporous silica SBA-15. J. Phys. Chem. B 110, 24450–24456.

Hashem, A.M., Abuzeid, H.M., Narayanan, N., Ehrenberg, H., Julien, C.M., 2011. Structural and electrochemical properties of α-MnO_2 doped with cobalt. Mater. Chem. Phys. 130, 32–38.

Koriche, N., Bouguelia, A., Mohammedi, M., Trari, M., 2007. Synthesis and physical properties of new oxide $AgMnO_2$. J. Mater. Sci. 42, 4780–4784.

LeVeque, R.J., Yee, H.C., 1990. A study of numerical methods for hyperbolic conservation laws with stiff source terms. J. Comput. Phys. 86, 187–210.

Li, H., Bian, Z., Zhu, J., Zhang, D., Li, G., Huo, Y., Li, H., Lu, Y., 2007. Mesoporous titania spheres with tunable chamber structure and enhanced photocatalytic activity. J. Am. Chem. Soc. 129, 8406–8407.

Liang, H.G., Qiu, X.P., Chen, H.L., He, Z.Q., Zhu, W.T., Chen, L.Q., 2004. Analysis of high rate performance of nanoparticled lithium

cobalt oxides prepared in molten KNO_3 for rechargeable lithium-ion batteries. Electrochem. Commun. 6, 789–794.
Lou, X.W., Archer, L.A., Yang, Z., 2008. Hollow micro-/nanostructures: synthesis and applications. Adv. Mater. 20, 3987–4019.
Ma, R.Z., Bando, Y., Zhang, L.Q., Sasaki, T., 2004. Layered MnO_2 nanobelts: hydrothermal synthesis and electrochemical measurement. Adv. Mater. 16, 918–922.
Ma, S.B., Nam, K.W., Yoon, W.S., Yang, X.Q., Ahn, K.Y., Oh, K.H., Kim, K.B., 2007. A novel concept of hybrid capacitor based on manganese oxide materials. Electrochem. Commun. 9, 2807–2811.
Ma, M.Y., Zhu, Y.J., Li, L., Cao, S.W., 2008. Nanostructured porous hollow ellipsoidal capsules of hydroxyapatite and calcium silicate: preparation and application in drug delivery. J. Mater. Chem. 18, 2722–2727.
Ma, J., Yang, J., Jiao, L., Wang, T., Lian, J., Duan, X., Zheng, W., 2011. Bi_2S_3 nanomaterials: morphology manipulation and related properties. Dalton Trans. 40, 10100–10108.
Matsuo, Y., Miyamoto, Y., Fukutsuka, T., Sugie, Y., 2005. Cathode properties of birnessite type manganese oxide prepared by using vanadium xerogel. J. Power Sources 146, 300–303.
Messaoudi, B., Joiret, S., Keddam, M., Takenouti, H., 2001. Anodic behaviour of manganese in alkaline medium. Electrochim. Acta 46, 2487.
Nagaraju, G., Thipperudraiah, K.V., Chandrappa, G.T., 2008. Organic assisted hydrothermal route to MoO_2/HDA composite microspheres and their characterization. Mater. Res. Bull. 43, 3297–3304.
Nakayama, M., Tanaka, A., Sato, Y., Tonosaki, T., Ogura, K., 2005. Electrodeposition of manganese and molybdenum mixed oxide thin films and their charge storage properties. Langmuir 21, 5907–5913.
Ragupathy, P., Vasan, H.N., Munichandraiah, N., 2010. Microwave driven hydrothermal synthesis of $LiMn_2O_4$ nanoparticles as cathode. Material for Li-ion batteries. Mater. Chem. Phys. 124, 870–875.
Sawangphruk, M., Pinitsoontorn, S., Limtrakul, J., 2012. Surfactant-assisted electrodeposition and improved electrochemical capacitance of silver-doped manganese oxide pseudocapacitor electrodes. J. Solid State Electrochem. 16, 2623–2629.
Thackeray, M.M., 1997. Manganese oxides for lithium batteries. Prog. Solid State Chem. 25, 1–71.
Tsuda, M., Arai, H., Sakurai, Y., 2002. Improved cyclability of Na-birnessite partially substituted by cobalt. J. Power Sources 110, 52–56.
Vries, A.H., Hozoi, L., Broer, R., Bagus, P.S., 2002. Importance of interatomic hole screening in core-level spectroscopy of transition metal oxides: Mn 3s hole states in MnO. Phys. Rev. B 66, 035108–035118.
Wingert, P.A., Mizukami, H., Ostafin, A., 2007. Enhanced chemiluminescent resonance energy transfer in hollow calcium phosphate nanoreactors and the detection of hydrogen peroxide. Nanotechnology 18, 295707–295713.
Wu, C.Z., Xie, Y., Lei, L.Y., Hu, S.Q., OuYang, C.Z., 2006. Synthesis of new-phased VOOH hollow dandelions and their application in lithium-ion batteries. Adv. Mater. 18, 1727–1732.
Yang, X., Tang, W., Liu, Z., Makita, Y., Kasaishi, S., Ooi, K., 2002. Co-precipitation synthesis of acetylene black/Li-birnessite composite suitable for a Li-rechargeable battery. Electrochem. Solid-State Lett. 5, A191–A194.
Yin, H., Feng, X.H., Qiu, G.H., Tan, W.F., Liu, F., 2011. Lead adsorption and arsenite oxidation by cobalt doped birnessite. J. Hazard. Mater. 188, 341–349.
Yu, H., Yu, J., Cheng, B., Liu, S., 2007. Novel preparation and photocatalytic activity of one-dimensional TiO_2 hollow structures. Nanotechnology 18, 065604–065611.
Zeng, S., Tang, K., Li, T., Liang, Z., Wang, D., Wang, Y., Zhou, W., 2007. Facile route for the fabrication of porous hematite nanoflowers: its synthesis, growth mechanism, application in the lithium ion battery, and magnetic and photocatalytic properties. J. Phys. Chem. C 111, 10217–10225.
Zhang, G.-Q., Zhang, X.-G., Wang, Y.-G., 2004. Anew air electrode based on carbon nanotubes and Ag–MnO_2 for metal air electrochemical cells. Carbon 42, 3097–3102.
Zhao, Q., Gao, Y., Bai, X., Wu, C., Xie, Y., 2006. Facile synthesis of SnO_2 hollow nanospheres and applications in gas sensors and electrocatalysts. Eur. J. Inorg. Chem. 8, 1643–1648.
Zheng, H., Feng, C., Kim, S.-J., Yin, S., Wua, H., Wang, S., Li, S., 2013. Synthesis and electrochemical properties of KMn_8O_{16} nanorods for lithium ion batteries. Electrochim. Acta 88, 225–230.
Zhu, Y., Shi, J., Shen, W., Dong, X., Feng, J., Ruan, M., Li, Y., 2005. Uniform magnetic hollow spheres with a magnetic core/mesoporous silica shell structure. Angew. Chem. Int. Ed. 44, 5083–5087.
Zhu, H.T., Luo, J., Yang, H.X., Liang, J.K., Rao, G.H., Li, J.B., Du, Z.M., 2008. Synthesis and magnetic properties of antiferromagnetic Co_3O_4 nanoparticles. J. Phys. Chem. C 112, 17089–17094.